Journal of Magnetic Resonance 237 (2013) 79–84

Contents lists available at ScienceDirect

Journal of Magnetic Resonance

journal homepage: www.elsevier.com/locate/jmr

A cryogenic receiver for EPR

R. Narkowicz [a,*], H. Ogata [b], E. Reijerse [b], D. Suter [a]

[a] Department of Physics, TU Dortmund University, Otto-Hahn-Str. 4, D-44221 Dortmund, Germany
[b] Max-Planck Institute for Chemical Energy Conversion, Stiftsraße 34-36, D-45470 Mülheim a.d. Ruhr, Germany

ARTICLE INFO

Article history:
Received 18 June 2013
Revised 24 September 2013
Available online 10 October 2013

Keywords:
Cryogenic receiver
Planar microresonators
Signal-to-noise ratio
Sensitivity

ABSTRACT

Cryogenic probes have significantly increased the sensitivity of NMR. Here, we present a compact EPR receiver design capable of cryogenic operation. Compared to room temperature operation, it reduces the noise by a factor of ≈2.5. We discuss in detail the design and analyze the resulting noise performance. At low microwave power, the input noise density closely follows the emission of a cooled 50 Ω resistor over the whole measurement range from 20 K up to room temperature. To minimize the influence of the microwave source noise, we use high microwave efficiency (≈1.1–1.7 mT $W^{-1/2}$) planar microresonators. Their efficient conversion of microwave power to magnetic field permits EPR measurements with very low power levels, typically ranging from a few μW down to fractions of nW.

1. Introduction

The increase of the Boltzmann factor at low temperature enhances the sensitivity of electron spin resonance (EPR) compared to room-temperature. The lower sample temperature can also lead to saturation and to a reduction of the signal intensity. Independent of the sample, it is possible to further increase the signal to noise ratio by cooling not only the sample, but also the relevant components of the detector and thereby reduce the thermal noise that limits the sensitivity. This approach has been used successfully in "cold probes" for NMR [1–3], but very little in EPR. Cryogenically cooled resonators and preamplifiers were used in [4,5] to investigate interfaces and defects in semiconductors by means of EPR. Both teams used home-built X-band spectrometers with a single-sideband superheterodyne detection at an intermediate frequency of 30 MHz to suppress the image microwave noise. A high-frequency (128 GHz) heterodyne microwave bridge, operating at the temperature of 1.5 K, was described in [6] with application to atomic hydrogen gas. In-depth analysis of advantages of cooling down a resonator and a preamplifier in the homodyne EPR spectrometer was performed in [7]. Using the concept of the equivalent noise temperature, the authors evaluated the dependence of the spectrometer noise on its construction and suggested ways to improve its signal-to-noise ratio. They emphasized the importance of cooling the load resistor on the excitation input of the circulator, while the circulator itself remained at room temperature, and proposed to suppress the influence of the microwave source noise by using loop-gap resonators with a low quality factor. Cooling down all major components of the receiver, including the circulator, was implemented as one of the signal amplification options in [8]. In their pulsed S-band EPR spectrometer, the authors installed the resonator, cryogenic circulator and microwave preamplifier in the cryostat. Based on the quantitative analysis of signal and noise in the EPR spectrometer, they concluded that a configuration in which all these components are in close proximity and are all cooled should yield the best signal-to-noise.

In this paper, we demonstrate the power of this approach. Our setup combines a cryogenic preamplifier with a magnetically shielded circulator and a resonator working at cryogenic temperatures. The spectrometer has been optimized for CW EPR, which allows to omit the protection circuit for the preamplifier, whose losses would degrade the signal-to-noise ratio of the spectrometer. Pulsed excitation with low microwave power should still be possible.

In our setup, we use planar microresonators, optimized for nanoliter-sized samples. Several probes, designed to measure EPR of limited-size samples at low temperatures using either miniature loop-gap resonators [9–11] or microstrip resonators with standard metallization [12], as well as superconducting traces [13,14] were demonstrated recently. High sensitivities of these structures at low temperatures are achieved both through optimized design of the probes and the gain in the Boltzmann factor. Here we investigate an additional sensitivity gain due to the reduced thermal noise of the cooled preamplifier.

Our microresonatos have high microwave-to-magnetic field conversion efficiency, which allows us to perform the experiments at very low microwave power. We investigate the dependence of the signal and noise of our receiver on the temperature and present

* Corresponding author. Fax: +49 231 755 3516.
E-mail address: rysard.narkovic@uni-dortmund.de (R. Narkowicz).

1090-7807/$ - see front matter © 2013 Elsevier Inc. All rights reserved.
http://dx.doi.org/10.1016/j.jmr.2013.09.017

results of the EPR measurements performed with the nanoliter-sized samples at cryogenic temperatures.

2. Experimental setup

For the experiments described here, we designed and constructed the setup shown in Fig. 1. The homodyne spectrometer is operated in reflection mode at a frequency of 14 GHz, corresponding to a resonant magnetic field of ≈500 mT. The microwave oscillator (1) working at room temperature feeds the excitation arm and the local oscillator port of the quadrature mixer (7) via the reference arm. The most critical components of the receiver are the circulator (5) and preamplifier (6), which are mounted in the variable temperature insert of the cryostat (Oxford Spectromag, 3T) at a distance of ≈20 cm from the resonator. The superconducting coils in the cryostat provide the static magnetic field $\mathbf{B}_0$ for the CW EPR experiments. The circulator is protected by a μ-metal shield against magnetic fields of up to 150 mT. We therefore placed it at a position where the field strength is ≈10% of the maximum. At the $g = 2$ resonance of our spectrometer, this results in 50 mT. The input port of the circulator is protected from the room temperature noise by a cooled 10 dB attenuator.

For the EPR measurements we used planar microresonators (PMRs) [15], such as the one shown in Fig. 2. The resonators were manufactured by copper electrodeposition on a TMM10i substrate (Rogers Corp). Due to the excellent thermal stability of its dielectric constant and the geometric parameters, the resonance frequency of the resonator remained quite stable over the whole range of temperatures used in our experiments. We observed a frequency shift of the resonance from 13.6 GHz at room temperature to 13.73 GHz at 10 K.

Small grain of DPPH was placed into a 200 μm loop of an R-shaped PMR (Fig. 2). Other samples were inserted into the via hole in the 500 μm loop of the Ω-shaped PMR using the 400 μm outer diameter, 300 μm inner diameter quartz capillaries. Measured microwave efficiency values for both types of resonators were 1.7 mT $W^{-1/2}$ and 1.1 mT $W^{-1/2}$ respectively [16]. Nutation measurements with N@C60 sample at room temperature and at 10 K in 500 μm PMR as well as the simulations using the finite element method (HFSS V.15, ANSYS) did not show a significant variation of the microwave efficiency with temperature.

For the temperature measurements, we used three temperature sensors: a Cernox sensor at the bottom of the variable temperature insert, a ruthenium oxide sensor just above the resonator, and an AlGaAs diode sensor on the preamplifier.

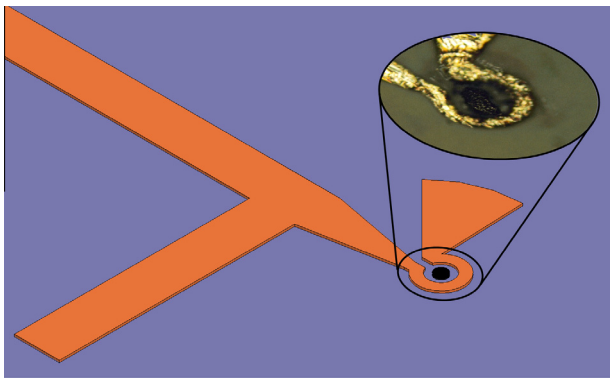

Fig. 2. Layout of the R-shaped planar microresonator with DPPH grain in the loop. The 200 μm loop is tuned with the radial stub and matched with the rectangular stub to achieve optimal coupling at the operation frequency. It is connected to the input of a circulator via the microstripline with the coaxial connector (not shown). A photograph in the inset reveals a grain of the DPPH in the loop of PMR. The sample volume estimated from the photograph is $(160 \times 80 \times 60)\ \mu m^3$.

3. Receiver gain

We first calibrated the gain G_R of the cryogenic receiver as a function of temperature. For this, we injected a calibrated signal whose frequency was offset by 100 kHz from the 14 GHz reference frequency. This reference frequency was far enough from the resonator dip, so it was fully reflected by the resonator connected to the circulator port 2 and appeared at the input of the preamplifier. The losses of the individual sections of the spectrometer and the gains of the active components (at room temperature) were measured with a network analyzer (Anritsu 54100A). The downconverted signal at 100 kHz was measured with the same lock-in amplifier as the actual EPR signal. The dependence of the output power on the input was then recorded to obtain the system gain value as a function of temperature. The same procedure was applied to the quadrature mixer and videoamplifiers to calibrate their gain at room temperature. Fig. 3 shows the results of the end-to-end receiver gain measurements.

At room temperature, the difference between the gain of the preamplifier and the overall gain of the receiver is 19.5 dB. If we assume that the loss of the passive components in the cryostat does not depend on temperature, we can determine the temperature dependence of the preamplifier gain by subtracting 19.5 dB from the overall gain of the receiver. The result is shown as the green curve in Fig. 3.

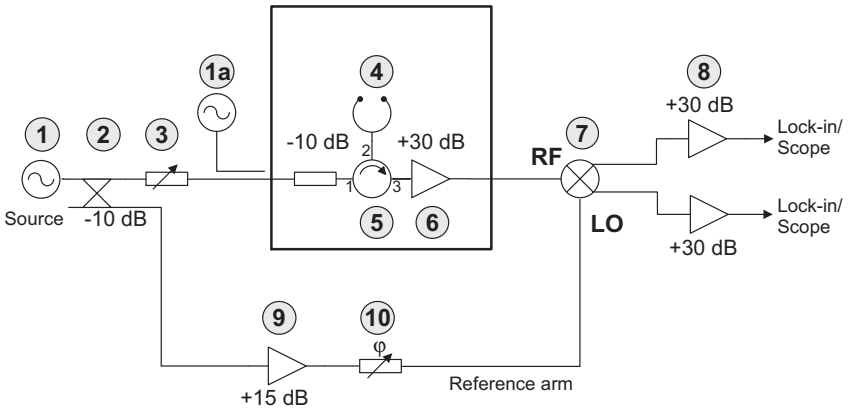

Fig. 1. Setup for EPR signal, gain and noise measurements as a function of temperature: (1) microwave oscillator Miteq OTC-1CM-134-141-15P-AFC or (1a) microwave generator Agilent E8257D, used for gain calibration, (2) directional coupler MCLI C7-10, (3) level set attenuator Alan 50CA 14,8-2118, (4) planar microresonator, (5) cryogenic circulator Pamtech PTC1408KS, (6) cryogenic preamplifier AFS4-12801480-05-CR-4, (7) quadrature mixer Anaren 250129, (8) videoamplifiers Miteq AU-1310, (9) amplifier AL28-13.4-14.1-12, and (10) phaseshifter Arra 9426B. Isolators and DC blocks are omitted for clarity.

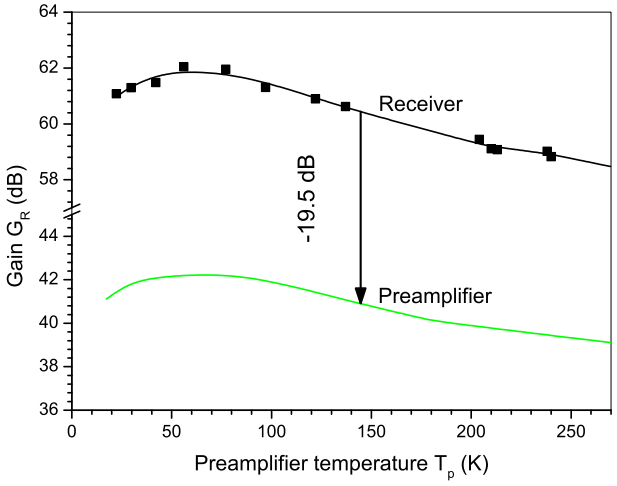

Fig. 3. Receiver gain as a function of the preamplifier temperature. The black squares represent the experimental data and the black line represent a polynomial fit to the measured data. The green line shows the preamplifier gain (in dB) as a function of temperature, obtained from the total gain under the assumption that the gain and losses of the other components do not change with temperature. (For interpretation of the references to color in this figure legend, the reader is referred to the web version of this article.)

4. Signal calculation

The voltage ϵ induced in the loop of the PMR by the precessing magnetization **M** can be calculated using the principle of reciprocity [17,18]:

$$\epsilon(t) = -\int \frac{d}{dt}(\mathbf{B}_{1u}(\mathbf{r}) \cdot \mathbf{M}(\mathbf{r},t))dV_s, \tag{1}$$

where $\mathbf{B}_{1u}(\mathbf{r}) = \mathbf{B}_{1r}(\mathbf{r})/I_0$ is the magnetic field B_{1r} at the position **r** produced by a unitary current I_0 carried by the loop of the microresonator and $\mathbf{M}(\mathbf{r},t)$ is the magnetization at this position. If we assume B_{1u} to be constant over the sample volume, slow passage conditions far from saturation ($(\gamma_e B_{1r})^2 T_1 T_2 \ll 1$), with T_1 and T_2 longitudinal and transverse relaxation times, the amplitude of the absorption signal is [19]:

$$\varepsilon_0 = \frac{2B_{1r}}{\Delta B} M_0 \omega_0 B_{1u} V_s. \tag{2}$$

Here ΔB is the full width at half height of the EPR line, ω_o is the EPR resonance frequency, V_s is the sample volume and M_0 is the static equilibrium magnetization

$$M_0 = \frac{n\gamma_e^2 \hbar^2 S(S+1)B_0}{3k_B T}, \tag{3}$$

n is the number of spins at resonance per unit volume, γ_e is the gyromagnetic ratio of the electron, k_B is the Boltzmann constant, S is the electron spin, and T is the sample temperature.

The signal generated in the loop is then coupled to the 50 Ω line. Taking into account the transformation coefficient of the tuning and matching circuit of the PMR and the transmission line connecting it to the input of the preamplifier, we obtain the signal at the receiver input as

$$S_{in} = \frac{\sqrt{\beta}}{1+\beta}\sqrt{\frac{Z_0}{r}}\varepsilon_0. \tag{4}$$

Here $Z_0 = 50\,\Omega$ is the impedance of the transmission line, r represents ohmic losses in the PMR and $\beta = 1/\mathrm{VSWR}$ is the coupling coefficient of the undercoupled resonator, and VSWR is the standing wave ratio.

To compare the absorption signal of Eq. (4) with the experimental peak-to-peak amplitude of the derivative-shape absorption curve, we calculate the amplitude of the component that oscillates at the modulation frequency as $c_1 = 0.42$ [20] when the magnetic field modulation amplitude B_m is equal to the peak-to-peak linewidth of the derivative signal ΔB_{pp}. As a result, the amplitude of the derivative spectrum is

$$\Delta S_{pp} = \frac{3}{2} c_1 S_{in}. \tag{5}$$

The unitary magnetic field B_{1u} in the loop can be determined from the microwave efficiency of the PMR, defined as $\Lambda = B_{1r}/\sqrt{P_{\mu w}}$, whee $P_{\mu w}$ stands for microwave power, which can be measured in a nutation experiment. Using the relation $P_{\mu w} = I_0^2 r/2$, we can express the unitary magnetic field as $B_{1u} = \Lambda\sqrt{r/2}$. Inserting Eqs. (2)–(4) into (5) we finally obtain the RMS voltage $U_{res} = (\Delta S_{pp})_{RMS}$, induced at the input of the preamplifier by the precessing magnetization as

$$U_{res} = \frac{\sqrt{\beta}}{1+\beta}\frac{\sqrt{3}}{2} c_1 \frac{\Lambda^2}{\Delta B_{pp}} \omega_0 M_0 V_s \sqrt{Z_0 P_{\mu w}}, \tag{6}$$

where $\Delta B_{pp} = \Delta B/\sqrt{3}$. This is the signal at the output of the resonator. The cables and the circulator connecting the PMR to the preamplifier attenuate the signal by ≈1.1 dB ($G \approx 0.88$), while the receiver has a gain G_R, leading to the output voltage

$$U_{out} = \sqrt{G_R} U_{in} = \sqrt{G_R} 0.88 U_{res}. \tag{7}$$

5. Noise

We quantify the sensitivity of the receiver by the signal-to-noise ratio. We therefore calculate the noise power at the output of the receiver by describing the matched resonator at resonance as a 50 Ω resistor. It radiates a noise power $P_{n,0} = k_B T \Delta f$, where T is the physical temperature of the resonator and Δf is the spectrometer bandwidth. Then the output noise power is [21]

$$P_{n,out} = G_R P_{n,0} + P_{n,R}, \tag{8}$$

where G_R stands for the receiver gain, starting at the input port of the cold preamplifier, and $P_{n,R}$ is the noise power added by the receiver. The dominant contribution to this term comes from the preamplifier and can be calculated as

$$P_{n,R} = G_R k_B T_{e,p} \Delta f, \tag{9}$$

where $T_{e,p}$ is the equivalent noise temperature of the preamplifier. In the factory test results for the preamplifier the manufacturer specifies a noise temperature of 115 K when the preamplifier is at room temperature, and 35 K when the preamplifier is cooled to 77 K. At lower temperatures, the noise temperature does not drop considerably below 35 K due to the power dissipated in the amplifier. Therefore for the intermediate temperatures, we use the interpolation function $T_{e,p} = 32\ \mathrm{K} + 10^{-3}\ \mathrm{K}^{-2}\ \mathrm{T}^2$. The noise power can be converted to noise voltage

$$U_{n,out} = \sqrt{Z_0 P_{n,out}}. \tag{10}$$

An extended calculation of the receiver noise from the equivalent noise temperature of a cascaded system, following an approach of Ref. [7], does not substantially alter the result of Eq. (8). For these calculations we use measured gains and losses of the setup components from the Table 1 in the Appendix and take into account the noise of all components in the receiver, as well as the noise from the excitation arm due to imperfect matching of the resonator. Due to the small reflections of the resonator at resonance as well as the presence of the cooled 10 dB attenuator at the input of the

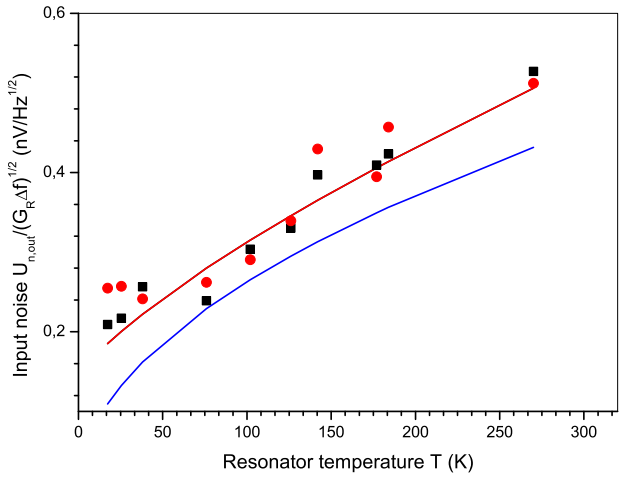

Fig. 4. Measured and calculated input noise voltage spectral density as a function of the resonator temperature. The blue curve is the thermal noise of a 50 Ω resistor, the red curve represents Eq. (10), which includes the noise of the cold preamplifier, and the squares and circles correspond to the experimental noise spectral densities measured on both channels of the receiver. The measurement setup is shown in Fig. 1.

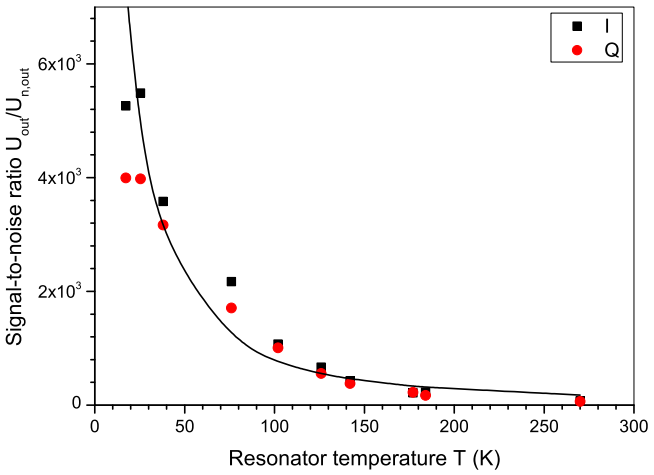

Fig. 5. Signal-to-noise ratio of the absorption (I) and dispersion (Q) signal of the cryogenic receiver. The solid line represents the signal-to-noise calculated from Eqs. (7) and (10), squares and circles denote experimental values, obtained from the microresonator with a DPPH sample at the excitation power of 20 pW. Modulation of $B_m = 1.9$ G was applied at the frequency of $f_m = 100$ kHz. The spectra were measured with the lock-in integration time of $\tau = 0.3$ s in a single sweep. The frequency varied with temperature from 13.6 to 13.73 GHz.

circulator, the additional noise does not exceed 1% of the noise calculated with our simplified approach.

The experimental spectrometer noise was measured at the lock-in inputs over the bandwidth of 0.4 Hz, corresponding to the lock-in integration time of 0.3 s, by off-resonant scanning of the static magnetic field during the EPR experiments. Input noise values in both channels were compared with the noise of the 50 Ω resistor.

Fig. 4 summarizes the temperature dependence of the noise. The blue curve $\propto \sqrt{T}$ shows the thermal noise of the resonator, which represents the theoretical limit. The red curve takes the preamplifier noise into account and the squares and circles represent the experimental data points measured by the lock-in of the spectrometer. Cooling the receiver from 270 K down to 17 K reduces the noise by a factor of ≈2.5. Given the simple model used for the calculation, the agreement between theory and experiment appears quite gratifying.

6. EPR measurements

6.1. DPPH

For the EPR measurements we used small grain of DPPH, with a volume of 7.7×10^{-7} cm^3 = 0.77 nl (Fig. 2). The spin density of DPPH is 2×10^{21} cm^{-3} [19], thus the sample contains 1.5×10^{15} spins. At the temperature of 213 K with the microwave power of 20 μW and modulation of 1.9 G, equal to the natural linewidth of the DPPH line, we achieved a sensitivity of 9.6×10^9 spins G^{-1} - Hz$^{-1/2}$. For microwave powers up to 1 mW, the receiver noise did not depend on the excitation power. Thus further reduction of this detection limit by a factor of ≈4 is possible by increasing the power up to the saturation level of ≈1 mW. Over the whole temperature range, a single line was observed.

As the temperature decreases below 25 K, the antiferromagnetic interaction between the spins leads to shorter transverse relaxation times and therefore to a noticeable line-broadening [22,23]. This is in agreement with earlier measurements [24,25], which report for DPPH in crystalline form $T_2 \approx 60$ ns at room temperature and decreasing to ≈20 ns at 4 K, while T_1 is of the order of 100 ns and remains almost constant down to 20 K. Below 25 K resonator temperature, the antiferromagnetic interaction also leads to a deviation of the signal amplitude from the Boltzmann law expected for paramagnetic materials [26].

EPR measurements with the DPPH sample were performed using very low excitation power (20 pW) over the whole range of measurement temperatures. Due to the very low excitation power and modulation width, the output noise was essentially thermal, with no detectable excess noise. Fig. 5 summarizes the experimental data and compares them to the theoretical function. The signal was measured as peak-to-peak distance in the derivative of absorption data and divided by the RMS noise. The measured signal-to-noise ratio at the resonator temperature of 25 K exceeds the value at room temperature by a factor of 70.

6.2. Cu/Ni dithiocarbamate crystal

To further investigate the performance of the spectrometer, we measured the EPR spectrum of a small crystal of Cu (II) doped Ni dithiocarbamate, Cu:Ni $(dtc)_2$. The sample was inserted into a 400 μm outer diameter, 300 μm inner diameter quartz capillary, sealed on both ends with wax. The capillary was inserted into the hole in the loop of the 500 μm Ω-shaped microresonator. The sample did not fill the "active" volume of the PMR of ≈35 nl completely. We approximated its volume of 1.4×10^{-5} cm^3 = 14 nl by a sphere with a diameter of 300 μm. The Ni $(dtc)_2$ crystal was doped with ≈1% Cu. The molar mass of this sample is 472 g/mol and the density 1.294 g/cm^3. It therefore contains 2.3×10^{14} spins. The T_2 of the Cu:Ni $(dtc)_2$ sample is about 360 ns at room temperature, while T_1 is about 600 ns and increases up to 200 μs when cooled down to 25 K [27].

Fig. 6 shows a typical spectrum, which contains two sets of four lines in the range of 450–490 mT. Several lines show splittings, with larger splittings on the outer lines of every set. The host crystal has the space group $P2_{1/c}$ with two magnetically inequivalent molecules per unit cell. Since the copper-containing molecules have the structure of the nickel complex, this gives rise to two copper hyperfine quartets [28]. All lines are partially split due to naturally occurring ^{63}Cu and ^{65}Cu isotopes with the same nuclear spin, but with slightly different magnetic moments.

The observed linewidth was ≈4 G. To evaluate the performance of the receiver, spectra were taken at two different temperatures,

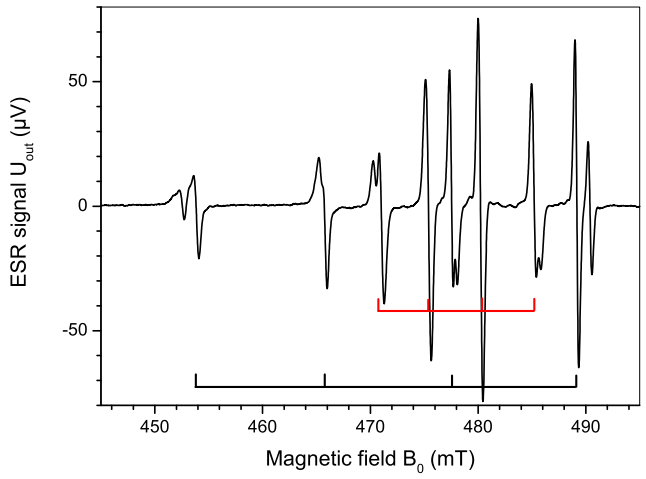

Fig. 6. EPR spectrum of the Cu:Ni $(dtc)_2$ sample, measured at a resonator temperature of 64 K, using a microwave power $P_{\mu w}$ = 2 μW at the frequency of $f_{\mu w}$ = 13.436 GHz. Magnetic field modulation of B_m = 2.1 G was applied at the frequency of f_m = 100 kHz and the lock-in integration time was τ = 0.3 s. Two copper hyperfine quartets are marked in black and red. (For interpretation of the references to color in this figure legend, the reader is referred to the web version of this article.)

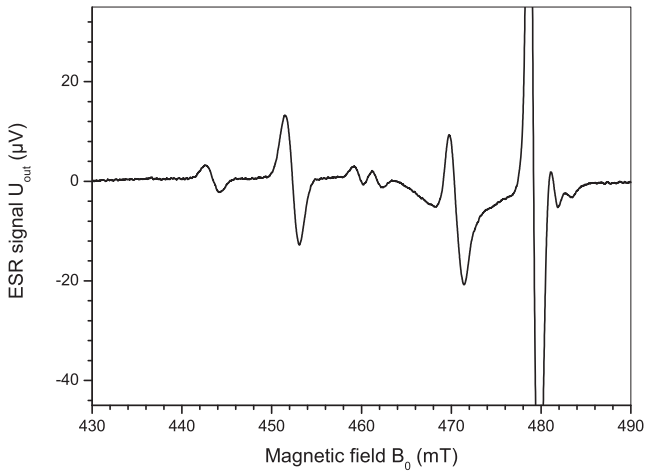

Fig. 7. EPR spectrum of the NiFe hydrogenase crystal, measured at the resonator temperature of 12 K using microwave power of $P_{\mu w}$ = 50 nW at the frequency of $f_{\mu w}$ = 13.428 GHz. Magnetic field modulation of B_m = 3.1 G was applied at the frequency of f_m = 100 kHz and lock-in integration time was τ = 0.3 s.

189 K and 64 K, reducing the microwave power from 20 μW down to 2 μW in order to avoid saturation. The signal-to-noise ratio was determined by comparing the signal at 480 mT with the RMS noise and was about 580 at 189 K and about 1300 at 64 K. This corresponds to the sensitivity of 1.8×10^{10} spins G^{-1} $Hz^{-1/2}$ at the temperature of 189 K and 8×10^9 spins G^{-1} $Hz^{-1/2}$ at the temperature of 64 K. Due to the saturation the signal amplitude of the strongest line increased not by the Boltzmann factor of ≈4, but by a factor of 1.4 only. Reduction of the noise by a factor of 1.6 contributed to the overall increase of the signal-to-noise ratio by a factor of 2.2.

6.3. NiFe hydrogenase

As a third test sample, we used a crystal of NiFe hydrogenase on which we performed EPR measurements at low temperatures (12 K and 62 K). Hydrogenases catalyze the reversible oxidation of molecular hydrogen (H_2). The majority of hydrogenases contain Ni, they are called NiFe hydrogenases [29]. The measured crystal of NiFe hydrogenase from Desulfovibrio vulgaris Miyazaki F had a needle – shape with a diameter of 200 μm. The crystal was inserted into a 300 μm inner diameter capillary and measured in a 500 μm Ω-shaped microresonator. The sample volume was thus a cylinder with 200 μm diameter and ≈350 μm length and a total volume of 1.1×10^{-5} cm^3 = 11 nl, compared to the 250 nl sample used in [29]. The unit cell of hydrogenase crystal has dimensions of $6.6 \times 10 \times 12.5$ nm^3 and four independent molecules per unit cell, thus the sample contains 5.3×10^{13} spins.

Fig. 7 shows the absorption spectrum. Isolated NiFe hydrogenases typically contain a mixture of two states: Ni-A ("unready") and Ni–B ("ready") [30]. Since there are four molecules in the unit cell, the fully-resolved spectrum of both paramagnetic states, Ni–A and Ni–B, contains eight lines. Hydrogenase from Desulfovibrio species contains also iron–sulfur clusters. The strong line of the [3Fe–4S] cluster near g = 2 may obscure part of the signals from the Ni-sites. The relaxation times of this sample are rather short: even at 5 K T_2 is only 360 ns for the [3Fe–4S] and 800 ns for the [NiFe] [31].

In our measurements, the signal of the [3Fe–4S] clusters at 480 mT increased strongly at T = 12 K. At low temperatures, the EPR signal of [NiFe] saturated at very low power levels, therefore the optimal power for maximum signal was changed from 5 μW at 62 K to 50 nW at 12 K. Due to the saturation the signal at 452.3 mT decreased by a factor of two, which was compensated by reduction of noise by the same factor. This resulted in the signal-to-noise ratio of ≈260 and the sensitivity of 5×10^9 spins G^{-1} $Hz^{-1/2}$. The input noise voltage spectral density changed from 0.53 nV $Hz^{-1/2}$ at T = 62 K to 0.3 nV $Hz^{-1/2}$ at 12 K and remained about twice as large as the value calculated at the minimal input power and weak modulation (Fig. 4). The excess noise can be attributed to the relatively strong modulation used in these measurements.

7. Conclusions

We have built and tested a cryogenic receiver that provides excellent signal-to-noise ratios over a wide temperature range. Compared to a room-temperature receiver, the noise is reduced by a factor of ≈2.5, without any penalty in terms of microwave performance or filling factor. The compact design fits into the variable temperature insert of the cryostat (Oxford Spectromag).

The setup was tested in CW operation, but pulsed operation at low power should also be possible. The 1 dB compression point of the preamplifier is 3 mW. If we use a 3 mW excitation pulse and a PMR with a 200 μm loop and a microwave efficiency of 1.7 mT $W^{-1/2}$, this corresponds to a $\pi/2$ pulse duration of 96 ns. Shorter pulse durations are possible, e.g. by using a 20 μm loop with a measured conversion factor of 19 mT $W^{-1/2}$ [16], which should result in $\pi/2$ pulses of ≈9 ns. Higher powers and correspondingly shorter pulses can obviously be used if we approach the damage threshold (20 mW) and take into account that only the reflected power (≈1%) reaches the preamplifier.

At optimal conditions of low excitation power and weak modulation the total input noise density closely follows the temperature dependence of a cooled 50 Ω resistor over the whole measurement range from 20 K up to room temperature. At a physical temperature of 20 K, the input noise density is ≈0.2 nV $Hz^{-1/2}$. This exceeds the thermal noise density at this temperature by a factor of 1.7. To minimize the influence of the microwave source noise, we use in our setup high microwave efficiency ($\Lambda \approx 1.1 - 1.7$ mT $W^{-1/2}$) planar microresonators. Their very efficient conversion of the microwave power into magnetic field permits experiments with very low power levels, typically ranging from a few μW down to fractions of nW. This reduces power dissipation in low temperature

Table 1
Gains and losses of sections of the spectrometer at room temperature. The losses between the circulator port 1 and the input of the preamplifier were obtained by subtracting the position 2 from the whole loss between the cryostat input and the preamplifier (−14.4 dB). The losses of the quadrature mixer were obtained by subtracting gain of the videoamplifier from the total gain of the quadrature mixer and videoamplifier.

Section	Nr	Gain
Microwave generator to cryostat	1	−1.2
Cable in cryostat and attenuator	2	−12.2
Port 1 of circulator to resonator	3	−1.1
Resonator to preamplifier input	4	−1.1
Cryogenic preamplifier	5	38.4
Preamplifier to cryostat output	6	−1.5
Cryostat to quadrature mixer	7	−1.6
Quadrature mixer	8	−9.9/−9.8
Videoamplifier	9	32.5

experiments and the influence of noise from the microwave source. Another important contribution to the total noise comes from the magnetic field modulation. Contributions of the microwave source noise, the radiofrequency interference and other environmental factors to the total noise should be carefully minimized in order to benefit from the extremely low noise of the cryogenic amplifiers at low temperatures.

Apart from quantitative measurements of signal and noise as a function of temperature with a standard DPPH test sample, we checked the performance of our receiver by measuring spectra of a ≈14 nl Cu:Ni $(dtc)_2$ sample and a ≈11 nl NiFe hydrogenase crystal at several temperatures from 190 K down to 12 K. The obtained spectra had signal-to-noise ratio of ≈1300 for the Cu:Ni $(dtc)_2$ sample and ≈260 for the NiFe hydrogenase. These results demonstrate the suitability of our cryogenic receiver, combined with the planar microresonator, for EPR measurements on small samples at low temperatures.

Acknowledgments

The authors thank Dr. Anton Savitsky for valuable discussions on the selection of the appropriate test samples and evaluation of the results of EPR measurements with Cu/Ni dithiocarbamate and NiFe hydrogenase. This work was supported by the Mercator Research Center Ruhr under Contract No. Pr-2011-0007 and by the DFG under Contract No. SU-192/30-1.

Appendix A

See Table 1.

References

[1] P. Styles, N. Soffe, C. Scott, D. Crag, F. Row, D. White, P. White, A high-resolution NMR probe in which the coil and preamplifier are cooled with liquid helium, J. Magn. Reson. 60 (1984) 397–404.
[2] P. Styles, N.F. Soffe, C.A. Scott, An improved cryogenically cooled probe for high-resolution NMR, J. Magn. Reson. 84 (1989) 376–378.
[3] H. Kovacs, D. Moskau, M. Spraul, Cryogenically cooled probes – a leap in NMR technology, Prog. Nucl. Magn. Reson. Spectrosc. 46 (2005) 131–155.
[4] H.E. Altink, T. Gregorkiewicz, C.A.J. Ammerlaan, Sensitive electron paramagnetic resonance spectrometer for studying defects in semiconductors, Rev. Sci. Instrum. 63 (1992) 5742–5749.
[5] W.J. Wallace, R.H. Silsbee, Microstrip resonators for electron-spin resonance, Rev. Sci. Instrum. 62 (1991) 1754–1766.
[6] S. Vasilyev, J. Järvinen, E. Tjukanoff, A. Kharitonov, S. Jaakkola, Cryogenic 2 mm wave electron spin resonance spectrometer with application to atomic hydrogen gas below 100 mK, Rev. Sci. Instrum. 75 (2004) 94–98.
[7] S. Pfenninger, W. Froncisz, J. Hyde, Noise analysis of EPR spectrometers with cryogenic microwave preamplifiers, J. Magn. Reson. 113 (1995) 32–39.
[8] G.A. Rinard, R.W. Quine, R. Song, G.R. Eaton, S.S. Eaton, Absolute EPR spin echo and noise intensities, J. Magn. Reson. 140 (1999) 69–83.
[9] Y. Twig, E. Suhovoy, A. Blank, Sensitive surface loop-gap microresonators for electron spin resonance, Rev. Sci. Instrum. 81 (2010) 104703.
[10] Y. Twig, E. Dikarov, W.D. Hutchison, A. Blank, Note: high sensitivity pulsed electron spin resonance spectroscopy with induction detection, Rev. Sci. Instrum. 82 (2011) 076105.
[11] Y. Twig, E. Dikarov, A. Blank, Cryogenic electron spin resonance microimaging probe, J. Magn. Reson. 218 (2012) 22–29.
[12] A.C. Torrezan, T.P.M. Alegre, G. Medeiros-Ribeiro, Microstrip resonators for electron paramagnetic resonance experiments, Rev. Sci. Instrum. 80 (2009) 075111.
[13] O. Benningshof, H. Mohebbi, I. Taminiau, G. Miao, D. Cory, Superconducting microstrip resonator for pulsed ESR of thin films, J. Magn. Reson. 230 (2013) 84–87.
[14] H. Malissa, D.I. Schuster, A.M. Tyryshkin, A.A. Houck, S.A. Lyon, Superconducting coplanar waveguide resonators for low temperature pulsed electron spin resonance spectroscopy, Rev. Sci. Instrum. 84 (2013) 025116.
[15] R. Narkowicz, D. Suter, R. Stonies, Planar microresonators for EPR experiments, J. Magn. Reson. 175 (2005) 275–284.
[16] R. Narkowicz, D. Suter, I. Niemeyer, Scaling of sensitivity and efficiency in planar microresonators for electron spin resonance, Rev. Sci. Instrum. 79 (2008) 084702.
[17] D. Hoult, R. Richards, The signal-to-noise ratio of the nuclear magnetic resonance experiment, J. Magn. Reson. 24 (1976) 71–85.
[18] D. Hoult, The NMR receiver: a description and analysis of design, Prog. Nucl. Magn. Reson. Spectrosc. 12 (1978) 41–77.
[19] G. Boero, M. Bouterfas, C. Massin, F. Vincent, P.-A. Besse, R.S. Popovic, A. Schweiger, Electron-spin resonance probe based on a 100 μm planar microcoil, Rev. Sci. Instrum. 74 (2003) 4794–4798.
[20] H. Wahlquist, Modulation broadening of unsaturated Lorentzian lines, J. Chem. Phys. 35 (1961) 1708–1710.
[21] G.A. Rinard, R.W. Quine, S.S. Eaton, G.R. Eaton, Frequency dependence of EPR signal intensity, 250 MHz to 9.1 GHz, J. Magn. Reson. 156 (2002) 113–121.
[22] P. Swarup, B.N. Misra, A note on the paramagnetic resonance of free radical, Z. Phys. 159 (1960) 384–387.
[23] W. Duffy, D. Strandburg, Paramagnetism of carbazyl and hydrazyl free radicals, J. Chem. Phys. 46 (1967) 456–464.
[24] B. Misra, S. Gupta, Temperature variation of relaxation time in free radical complexes, Acta Phys. Acad. Sci. Hung. 37 (1974) 347–353.
[25] G. Höcherl, H.C. Wolf, Zur Konzentrationsabhängigkeit der Elektronenspin-Relaxationszeiten von Diphenyl-Picryl-Hydrazyl in fester Phase, Z. Phys. 183 (1965) 341–351.
[26] D. Žilić, D. Pajić, M. Jurić, K. Molčanov, B. Rakvin, P. Planinić, K. Zadro, Single crystals of DPPH grown from diethyl ether and carbon disulfide solutions – crystal structures, IR, EPR and magnetization studies, J. Magn. Reson. 207 (2010) 34–41.
[27] S.S. Eaton, J. Harbridge, G.A. Rinard, G.R. Eaton, R.T. Weber, Frequency dependence of electron spin relaxation for three S = 1/2 species doped into diamagnetic solid hosts, Appl. Magn. Reson. 20 (2001) 151–157.
[28] E.J. Reijerse, M.L.H. Paulissen, C.P. Keijzers, An electron spin-echo envelope modulation study of ^{14}N nuclear hyperfine and quadrupole coupling in copper (II)/nickel (II) bisN, N-di-n-butyl-dithiocarbamate, J. Magn. Reson. 60 (1984) 66–78.
[29] C. Geßner, O. Trofanchuk, K. Kawagoe, Y. Higuchi, N. Yasuoka, W. Lubitz, Single crystal EPR study of the Ni center of NiFe hydrogenase, Chem. Phys. Lett. 256 (1996) 518–524.
[30] O. Trofanchuk, M. Stein, C. Geßner, F. Lendzian, Y. Higuchi, W. Lubitz, Single crystal EPR studies of the oxidized active site of [NiFe] hydrogenase from Desulfovibrio vulgaris Miyazaki F, J. Biol. Inorg. Chem. 5 (2000) 36–44.
[31] S.S. Eaton, G.R. Eaton, Measurements of interspin distances by EPR, in: B.C. Gilbert, M.J. Davies, D.M. Murphy (Eds.), Electron Paramagnetic Resonance, The Royal Society of Chemistry, vol. 19, 2004, pp. 318–337.